

Valence shell double photoionization of alkaline-earth atoms

A. S. Kheifets

Research School of Physical Sciences,

*The Australian National University, Canberra ACT 0200, Australia**

Igor Bray

ARC Centre for Matter-Antimatter Studies,

Murdoch University, Perth, 6150 Australia †

(Dated: December 13, 2006)

Abstract

We apply the convergent close-coupling (CCC) formalism to describe direct double photoionization (DPI) of the valence ns^2 shell of alkaline-earth atoms: beryllium ($n = 2$), magnesium ($n = 3$) and calcium ($n = 4$). We consider the range of photon energies below the onset of resonant and Auger ionization processes where the subvalent and core electrons can be treated as spectators. By comparing alkaline-earth atoms with helium, we elucidate the role of the ground state and final ionized state correlations in DPI of various quasi two-electron atoms.

*Electronic address: A.Kheifets@anu.edu.au; URL: <http://rsphysse.anu.edu.au/~ask107>

†Electronic address: I.Bray@murdoch.edu.au; URL: <http://atom.murdoch.edu.au>

I. INTRODUCTION

Theoretical and experimental studies of direct double photoionization (DPI) of atomic targets beyond helium gained considerable momentum in recent years. Direct DPI process, in contrast to its resonant or Auger counterparts, is driven entirely by many-electron correlations and therefore is ideally suited to study electron correlations in atoms. Alkaline-earth atoms are attractive targets for these studies because of their relatively simple quasi two-electron structure. In these atoms, the outer valence shell is well separated from the rest of the atom. Therefore, at relatively small photon energies, the inner core and subvalent electrons can be treated as “spectators” not taking direct part in photoionization of the outer valence shell. In this situation, DPI process in alkaline-earth atoms is similar to that in He except for a different radial structure of the target ns orbital and the influence of the distorting potential on the departing photoelectrons.

Beryllium is an archetypal quasi two-electron system in which the separation of the valence and core orbitals is very well pronounced both in the coordinate space: $\langle r \rangle_{1s} = 0.41$ a.u., $\langle r \rangle_{2s} = 2.65$ a.u. and in energy: $\epsilon_{1s} = 4.73$ a.u., $\epsilon_{2s} = 0.31$ a.u. Here the Hartree-Fock values of the mean electron radii and the one-electron energies are calculated using the computer code of Dylla et al. [1]. In addition to the simple electronic structure, beryllium has an extended energy range from its double-ionization threshold at 27.53 eV [2] up to around 115 eV in which resonant or Auger mechanisms do not contribute to DPI process.

The first experimental observation of the direct valence shell DPI of Be was reported by Wehlitz and Whitfield [3] who measured the double-to-single photoionization cross-section ratio between the photon energies of 32 and 80 eV. At about the same time, but independently, the theoretical ratio was reported by Kheifets and Bray [4] who employed a frozen core model and treated Be as a He-like target within the convergent close-coupling (CCC) formalism. A good agreement between theory and experiment was found in subsequent analysis of the data [5]. The CCC results were also later confirmed by HRM-SOW [6] and TDCC [7] calculations. Very recently, Wehlitz and collaborators [5, 8] studied DPI of Be below the photon energy of 40 eV with much improved statistics and energy resolution. The new set of data for the DPI cross-section was found in agreement with the CCC and TDCC calculations. Close examination of the experimental DPI cross-section near threshold revealed quite an unexpected oscillating structure which was at variance with the Wannier

law and attributed to the Coulomb-dipole field of the singly ionized target [9].

More interest in direct DPI of beryllium was generated by a recent theoretical study of the angular correlation in the two-electron continuum in the ground state and metastable He and other two-electron targets [10]. It was argued that because DPI near threshold would proceed mainly via electron-impact ionization of the singly ionized target, the width of the angular correlation function in DPI was determined by the Compton profile of the target electron bound to the singly-charged ion. This mechanism could explain a considerable narrowing of the angular correlation function in Be as compared to He. An alternative explanation of this effect was proposed by Citrini et al. [6] who attributed it to a stronger ground state correlation in beryllium as compared to helium.

Direct valence shell DPI in heavier alkaline earth atoms (Mg, Ca, Sr) is studied to a much lesser extent. Osawa et al. [11] announced their measurement of the double-to-single cross-section ratio σ^{++}/σ^+ for Ca and Sr in the photon energy range from the double ionization threshold (17.99 eV for Ca and 16.73 eV for Sr) to just below the lowest excited state of the subvalent shell (30 eV for Ca and 24.5 eV for Sr). These data, however, are still to be published. Direct DPI of Ca was studied by Beyer et al. [12] who measured the fully resolved triply-differential cross-section (TDCS) at equal energy sharing between the photoelectrons and observed a marked difference from similar data in He.

Theoretically, direct DPI from Mg and Ca was first studied by Ceraulo et al. [13] within the theoretical scheme which took into account the final-state electron correlation by introducing a Coulomb hole factor. However, this approach for He failed to provide even qualitative agreement with the experimental data. Kazansky and Ostrovsky [14] calculated direct DPI in Be, Mg, Ca and Sr by employing an extended Wannier ridge model and mimicking the ground state correlation by introducing a Coulomb hole in the initial state. This theory predicted a double hump angular correlation function (reduced TDCS in the author's terminology) for all studied atoms. This prediction was not confirmed in subsequent CCC calculations for Be [4].

Valence shell DPI was studied experimentally in the region of the giant $3p \rightarrow 3d$ resonance in Ca [15, 16] and $4p \rightarrow 4d$ resonance in Sr [17, 18]. The Ca measurements were analyzed in subsequent theoretical papers [14, 19, 20]. These studies, however, go beyond the scope of the present work.

In this paper, we concentrate on direct valence shell DPI of Be, Mg and Ca in the range

of photon energies from the threshold to the lowest excitation from the core (Be) or nearest subvalent shell (Mg and Ca). The motivation of this work is to study systematically a range of quasi two-electron atoms and to elucidate the role of the ground and final state correlations in DPI process. In particular, we want to shed more light on the issue of angular correlation width in the two-electron continuum. We present more evidence that the narrowing of the angular correlation width from light to heavy alkaline earth atoms is related to the shrinking ns orbital in the momentum space which corresponds to a more diffuse orbital in the coordinate space shielded from the nucleus by inner electrons.

In the present work, we use essentially the same theoretical scheme as was employed in our earlier calculation on Be [4]. Although some results for Be were reported previously, we feel it necessary to include beryllium in the present study for systematics and because a large amount of good quality experimental data became available thus enabling us to subject the theory to a more stringent test.

The body of the present paper is organized as follows. In Sec. II we give a brief outline of our theoretical model. In Sec. III A we present our results for the integrated, single and double, photoionization cross-sections. In Sec. III B and Sec. III C, we analyze the DPI amplitudes and fully differential photoionization cross-sections. In Sec. IV we conclude by summarizing our findings and presenting a unifying picture of DPI of alkaline earth atoms and helium

II. FORMALISM

A. Multiconfiguration Hartree-Fock ground state

We assume the LS coupling scheme and make the following configuration-interaction expansion of the $ns^2 \ ^1S$ ground state:

$$\Psi_0(\mathbf{r}_1, \mathbf{r}_2) = \sum_{l=0}^{l_{\max}} \sum_{m=n}^{n_{\max}} C_{ml} |\phi_{ml}(\mathbf{r}_1) \phi_{ml}(\mathbf{r}_2) : ^1S\rangle \quad (1)$$

Only diagonal ml^2 terms are included in (1) as is always the case for the MCHF ground state. This is so because a HF ground state is stable with respect to the one-electron-one-hole excitations and the first non-vanishing correction should be of the two-electron-two-hole type.

The coefficients in the MCHF expansion (1) are found by using the MCHF computer code [1]. The number of terms in the MCHF expansion is increasing until we are satisfied with the stability of the ground state energy and, more importantly, the asymptotic photoionization ratios taken in the limit of infinite photon energy:

$$R_m^\infty = \frac{\sigma_m}{\sigma^+ + \sigma^{2+}} \Big|_{\omega \rightarrow \infty} = \frac{c_m}{c} \quad , \quad R_\infty = \frac{\sigma^{2+}}{\sigma^+} \Big|_{\omega \rightarrow \infty} = \frac{c - \sum_m c_m}{\sum_m c_m} \quad , \quad (2)$$

where σ_m is a single photoionization cross-section corresponding to an m final ion state, and $\sigma^+ = \sum_{m=n}^\infty \sigma_m$ and σ^{2+} are the total single and double photoionization cross-sections. In Eq. (2), we introduce the following overlap integrals [21]:

$$c_m \propto \left| \langle \phi_{ms}^+ | \delta(\mathbf{r}_2) | \Psi_0 \rangle \right|^2 \quad , \quad c \propto \left| \langle \Psi_0 | \delta(\mathbf{r}_2) | \Psi_0 \rangle \right|^2 \quad (3)$$

where ϕ_{ms}^+ is the one-electron ms orbital of the singly charged ion.

Results for R_m^∞ and R_∞ are shown in the Table. For comparison, we also show the corresponding parameters for the ground state He. Although the limit of infinite photon energy has no physical meaning for valence shell photoionization, we may use the asymptotic ratios as indicators of the relative strength of various single and double photoionization channels at finite photon energies. In particular, Pattard [22] proposed a universal shape function which bridges the low-energy Wannier behavior with the high-energy Bethe-Born theory:

$$\frac{\sigma^{2+}}{\sigma^+}(E) = R_\infty \frac{E^\alpha (E + E_0)^{7/2}}{(E + E_1)^{7/2}} \quad (4)$$

where $\alpha = 1.056$ is the Wannier exponent and E_0 and E_1 are the fitting parameters. The shape function (4) was used successfully by Wehlitz et al. [5] to describe experimental double-to-single photoionization cross-section ratio in Be.

We see that the asymptotic ratio R_∞ is decreasing systematically from He to Ca. This is related to the fact that the overlaps between the corresponding orbitals bound to the neutral atom and the singly charged ion $\langle ns || ns^+ \rangle$ are increasing from He to Ca which, in turn, is related to the shielding action of the core. This increases the relative probability of the target electron to remain bound and, therefore, decreases the probability of the double photoionization. A monotonic decrease in asymptotic ratios R_∞ from He to Mg is actually translated into decreasing double-to-single ratios at finite photon energies as will be shown in the following sections. The only exception from this sequence is Ca which has the smallest asymptotic ratio but the largest double-to-single ratio at finite photon energies.

TABLE I: Ground state properties of helium and alkaline-earth atoms.

n	1	2	3	4
Atom	He	Be	Mg	Ca
Expansion	MCHF15	MCHF13	MCHF17	MCHF15
l_{\max}	4	3	4	4
n_{\max}	5	5	6	6
R_m^∞ $m = 1$	94.541			
2	4.469	94.578		
3	0.564	4.817	94.738	
4	0.188	0.374	4.741	94.928
5	0.086	0.114	0.330	4.645
6	0.047	0.051	0.098	0.279
7	0.029	0.028	0.043	0.080
8	0.019	0.017	0.023	0.035
R_∞	1.758	0.370	0.256	0.175
C_{ns^2}	0.996	0.954	0.965	0.959
$\Delta\text{IP}^{\text{HF}}/\text{IP}$, %	1.4	4.5	5.9	8.6
$\Delta\text{IP}^{\text{MCHF}}/\text{IP}$, %	0.01	0.48	1.9	4.1

Other entries in the Table serve to indicate the comparative strength of the ground state correlation in He and alkaline earth atoms. The coefficient C_{ns^2} is accompanying the leading ns^2 configuration in the MCHF expansion (1). Deviation of this coefficient from unity indicates the admixture of other configurations to non-correlated Hartree-Fock ground state. The ground state correlation can also be quantified in terms of the correlation energy or, more specifically, the relative shift of the theoretical Hartree-Fock double ionization potential with respect to the experimental one $\Delta\text{IP}^{\text{HF}}/\text{IP}$. By both counts, He is the least correlated atom which is bound tightly by the Coulomb force of the bare nucleus. As the nucleus becomes shielded, the strength of the ground state correlation is gradually increasing from Be to Ca.

The last entry in the table is the relative shift of the theoretical MCHF double ionization

potential with respect to the experimental one $\Delta\text{IP}^{\text{MCHF}}/\text{IP}$. It gives an indication of the accuracy of the MCHF expansion achieved with a given number of terms.

B. CCC Formalism

The photoionization cross section, as a function of the photon energy ω , corresponding to a particular bound electron state j of the ionized target is given by [23]

$$\sigma_j(\omega) = \frac{4\pi^2}{\omega c} \sum_{m_j} \int d^3k_b |\langle \Psi_j^{(-)}(\mathbf{k}_b) | \mathcal{D} | \Psi_0 \rangle|^2 \delta(\omega - E + E_0), \quad (5)$$

where $c \simeq 137$ is the speed of light in atomic units.

The dipole electro-magnetic operator \mathcal{D} can be written in the length or velocity gauges:

$$\mathcal{D}^r = \omega(\mathbf{r}_1 + \mathbf{r}_2) \cdot \hat{\mathbf{e}}, \quad \mathcal{D}^\nabla = (\nabla_1 + \nabla_2) \cdot \hat{\mathbf{e}}$$

Here $\hat{\mathbf{e}}$ is the polarization vector of the photon. The dipole matrix element entering Eq. (5) is calculated in the CCC formalism as

$$\begin{aligned} \langle \Psi_j^{(-)}(\mathbf{k}_b) | \mathcal{D} | \Psi_0 \rangle &= \langle \mathbf{k}_b^{(-)} j | \mathcal{D} | \Psi_0 \rangle \\ &+ \sum_i \int d^3k \frac{\langle \mathbf{k}_b^{(-)} j | T | i \mathbf{k}^{(+)} \rangle \langle \mathbf{k}^{(+)} i | \mathcal{D} | \Psi_0 \rangle}{E - \varepsilon_k - \varepsilon_i + i0}. \end{aligned} \quad (6)$$

Here the channel wave function $\langle \mathbf{k}_b^{(-)} j |$ is the product of a one-electron target orbital φ_j with energy ε_j and a (distorted) Coulomb outgoing wave $\chi^{(-)}(\mathbf{k}_b)$ with energy ε_k . Like in the case of helium, the target orbital is generated with the asymptotic charge being two, and the asymptotic charge seen by the Coulomb wave is one.

The square-integrable basis set of the target states ϕ_n^N is obtained by diagonalizing the target Hamiltonian H_T in a large Laguerre (Sturmian) basis of size N

$$\langle \varphi_m^N | H_T | \varphi_n^N \rangle = \epsilon_n^N \delta_{mn}. \quad (7)$$

The target two-electron Hamiltonian is defined as

$$H_T = \sum_{i=1,2} \left(-\frac{1}{2} \nabla_i^2 + V_i^{\text{FC}} + V_i^{\text{pol}} \right) + \frac{1}{|\mathbf{r}_1 - \mathbf{r}_2|} \quad (8)$$

The non-local frozen-core potential V^{FC} is generated by performing a self-consistent-field Hartree-Fock calculation [24] for the ground state of the doubly charged ion

$$V^{\text{FC}} \varphi_\alpha(\mathbf{r}) = \left(-\frac{Z}{r} + 2 \sum_{\varphi_j \in C} \int d^3r' \frac{|\varphi_j(\mathbf{r}')|^2}{|\mathbf{r} - \mathbf{r}'|} \right) \varphi_\alpha(\mathbf{r}) - \sum_{\varphi_j \in C} \int d^3r' \frac{\varphi_j^*(\mathbf{r}') \varphi_\alpha(\mathbf{r}')}{|\mathbf{r} - \mathbf{r}'|} \varphi_j(\mathbf{r}), \quad (9)$$

Here the polarization potential of the subvalent shell is

$$V^{\text{pol}}(r) = -\alpha_d/2r^4 W_6(r/\rho),$$

where

$$W_6(r/\rho) = \left\{ 1 - \exp \left[-(r/\rho)^6 \right] \right\},$$

and α_d is the static dipole polarizability.

The contribution from the final channels $\langle \mathbf{k}_b^{(-)} | j \rangle$ is separated into single and double ionization according to the energy ϵ_j which is positive for the double ionized channels and negative for the singly ionized channels. We also ensure that for the negative-energy state cross sections, contributions to the ionization plus excitation cross sections are multiplied by the projection of the state onto the true target discrete subspace as is done for electron-impact ionization [25].

The fully differential DPI TDCS is calculated from the dipole matrix element $\langle \Psi(\mathbf{k}_1, \mathbf{k}_2) | \mathcal{D} | \Psi_0 \rangle$ between the ground state and the two-electron continuum. This matrix element can be obtained from the set of matrix elements (6) by projecting the distorted wave $\langle \mathbf{k}_2^{(-)} |$ onto the target pseudostate of matching energy $\epsilon_j = k_2^2/2$ in all partial wave channels. It is convenient to parametrize the TDCS by a pair of symmetrized amplitudes $f^\pm(\theta_{12}, E_1, E_2)$ which depend on the relative interelectron angle and energy [26, 27]:

$$\frac{d^3\sigma}{d\Omega_1 d\Omega_2 dE_2} = \frac{4\pi^2 k_1 k_2}{\omega c} |\langle \Psi(\mathbf{k}_1, \mathbf{k}_2) | \mathcal{D} | \Psi_0 \rangle|^2 = \left| \left[f^+ (\hat{\mathbf{k}}_1 + \hat{\mathbf{k}}_2) + f^- (\hat{\mathbf{k}}_1 - \hat{\mathbf{k}}_2) \right] \cdot \hat{\mathbf{e}} \right|^2. \quad (10)$$

Here $\hat{\mathbf{k}}_i = \mathbf{k}_i/k_i$, $i = 1, 2$ are the unit vectors directed along the photoelectron momenta \mathbf{k}_i . Under the equal energy sharing condition, the anti-symmetric amplitude vanishes $f^-(E_1 = E_2) = 0$ and all the information about the DPI process is contained in one symmetric amplitude f^+ . Following predictions of the Wannier-type theories [28, 29], this amplitude can be represented by a Gaussian ansatz:

$$|f^+|^2 \propto \exp \left[-4 \ln 2 \frac{(\pi - \theta_{12})^2}{\Delta\theta_{12}^2} \right] \quad (11)$$

where the width parameter $\Delta\theta_{12}$ indicates the strength of angular correlation in the two-electron continuum. Although the analytical theories [28, 29] validate Eq. (11) only near the double ionization threshold, numerical models [30] and direct measurements [31, 32] support its validity in a far wider photon energy range.

The number of the states N in the Laguerre basis (7) was increased until satisfactory convergence was achieved. In practice, our calculations were performed with at least $45 - l$ target states where

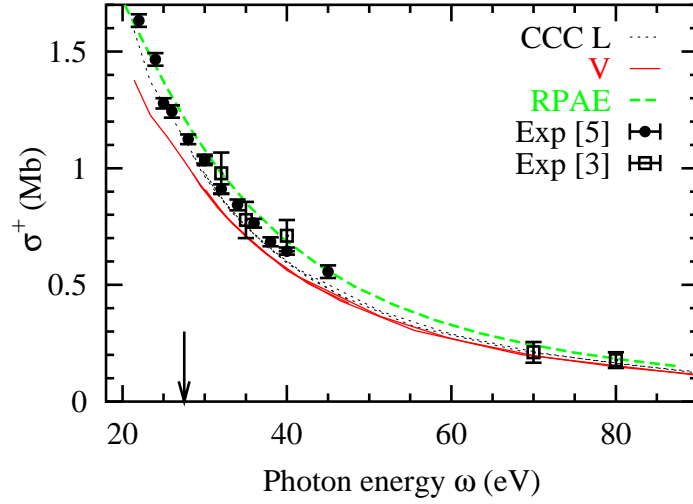


FIG. 1: Single photoionization cross-section of Be as a function of the photon energy. The CCC calculations in the length and velocity gauges are shown by the black dotted and red solid lines, respectively. The RPAE calculation in two gauges (indistinguishable) is shown by the green dashed line. Experimental data of Wehlitz et al. [5] and Wehlitz and Whitfield [3] are displayed by filled circles and open squares, respectively. The arrow indicates the double ionization threshold.

$l = 0, \dots, l_{\max}$ is the angular momentum of the target orbital and $l_{\max} = 8$. Higher values of the l_{\max} are required for alkaline earth atoms as compared with He because of a larger radial extent of the target orbitals bound to the corresponding singly charged ion.

III. RESULTS

A. Integrated cross-sections

1. Beryllium

In their recent paper, Wehlitz et al. [5] reported cross-section data for both single and double photoionization of Be from threshold to 40 eV photon energy range with improved statistics and energy resolution. This provides our CCC model with a stringent test case, not available at a time of our previous publication [4]. Therefore we feel it necessary to reexamine our earlier Be data in the present work.

In Figure 1 we present the single photoionization cross-section calculated in two gauges of the

electromagnetic interaction, the length and velocity. If the ground and final state wave functions were exact, these two calculations would produce identical results. In practice, there is some deviation between the two gauges, especially at low photon energies. We believe this deviation is due to the frozen core approximation employed in the present work. Indeed, by taking into account the inter-shell correlation between the $1s^2$ and $2s^2$ shells within the random phase approximation with exchange (RPAE) [23], we were able to produce identical results in both gauges even with a non-correlated ground state. Unfortunately, RPAE calculations can only be performed for single photoionization and cannot be used in the present DPI study.

Experimental data of Wehlitz et al. [5] are consistent with the present CCC calculation with a somewhat better agreement with the length gauge near the double ionization threshold. All calculations tend to converge further away from the threshold where they are in good agreement with the earlier measurement of Wehlitz and Whitfield [3].

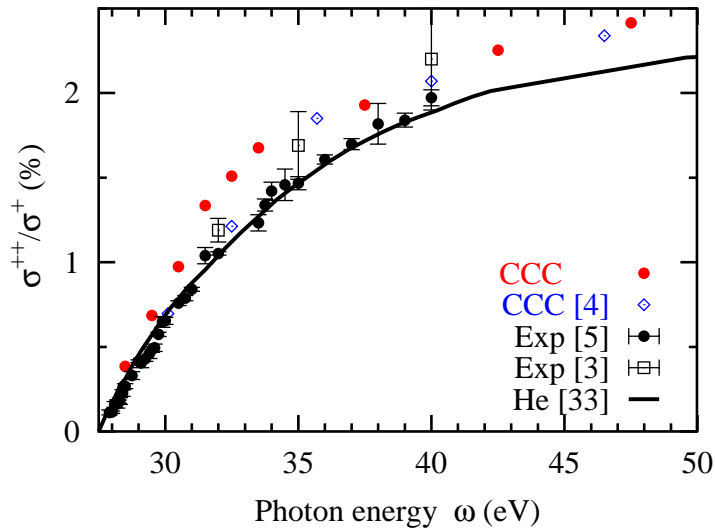


FIG. 2: Double-to-single photoionization cross-sections ratio in Be as a function of the photon energy. Present CCC calculation in the velocity gauge is plotted by red filled circles. Previous CCC results [4] are shown by blue open diamonds. Experimental data of Wehlitz et al. [5] and Wehlitz and Whitfield [3] are displayed by filled circles and open squares, respectively. The black thick solid line is the theoretical double-to-single ratio in He [33] multiplied by 0.64 and plotted versus the excess energy in units of the ionization potential of He^+ .

In Figure 2 we present the double-to-single photoionization cross-section ratio in Be. We plot the present CCC calculation in the velocity gauge along with an earlier calculation reported in Ref. [4].

CCC calculations in the length gauge are not reliable for alkaline earth atoms due to a poor quality of the MCHF ground state and are not shown in the figure. We compare the CCC calculations with the experimental data of Wehlitz et al. [5] and Wehlitz and Whitfield [3]. Wehlitz et al. [5] noticed that the experimental double-to-single ratio in Be can be scaled to the analogous ratio in He when plotted versus the excess energy ΔE in units of the ionization potential of the corresponding singly charged ion (Be^+ or He^+). Their reasoning was that the DPI near threshold should proceed mainly via the electron impact ionization of the singly charged ion. The cross-section of the former process is a universal function of the reduced excess energy for all hydrogen-like targets.

We adopt this scaling and compare in Figure 2 the CCC double-to-single ratios of Be and He in the reduced coordinates. We see that the scaled He calculation [33] agree very well with the Be experiment whereas the Be calculation is somewhat higher. To certain extent, this disagreement might be due to the reduced single photoionization cross-section in the velocity gauge clearly visible in Figure 1.

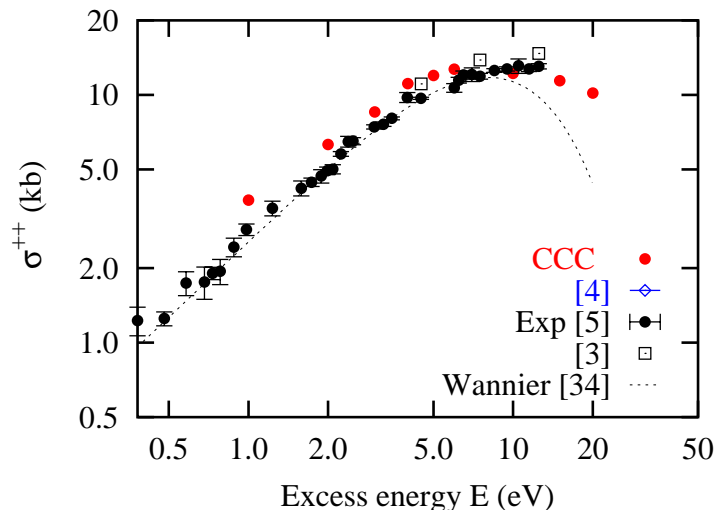


FIG. 3: Double photoionization cross-section of Be as a function of excess energy above the double ionization threshold. The captions are the same as in Figure 3 except for the dotted line which shows the fit of experimental data with the fourth-order Wannier theory [34]

To separate double and single photoionization more clearly, we plot in Figure 3 the absolute double photoionization cross-section of Be both from the CCC calculations and the experiments of Wehlitz' group. As in Ref. [5], the experimental data are fitted with the fourth order Wannier theory of Feagin [34]. The CCC calculation in the velocity gauge is generally consistent with

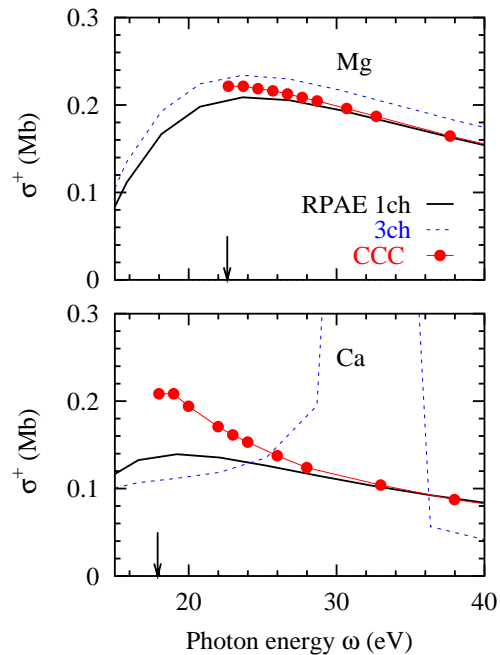


FIG. 4: Single photoionization cross-sections of Mg (top) and Ca (bottom) as a function of the photon energy. RPAE calculations with 1 and 3 channels are shown by the black solid and blue dashed lines, respectively. The 3-channel RPAE calculation for Ca is scaled down by a factor of 0.2. The CCC calculation is shown with the red circles. The corresponding double ionization thresholds are indicated by arrows.

the experimental data. However, the calculated cross-sections are systematically larger than the experiment at the excess energies below 10 eV.

2. Magnesium and calcium

Unlike Be, heavier alkaline earth atoms, Mg and Ca have a subvalent $(n - 1)p$ shell which can affect photoionization of the valence ns shell. This effect can be particularly strong in Ca due to proximity of the giant $3p \rightarrow 3d$ resonance at 31.4 eV to the double ionization threshold. We cannot account for inter-shell electron correlation in the presently employed frozen core model. However, we can examine this effect in the single photoionization channel where we can perform a separate RPAE calculation.

The single photoionization cross-sections of Mg and Ca near the corresponding double ionization threshold are presented in Figure 4. Three calculations are shown in the figure. In the one-channel RPAE calculation, only ionization of the valence shell $ns \rightarrow \epsilon p$ is taken into account. In a more

sophisticated RPAE calculation, the inter-shell electron correlation is taken into account by mixing three photoionization channels: $ns \rightarrow \epsilon p$ and $(n-1)p \rightarrow \epsilon s, \epsilon d$. In Mg, the difference between the two RPAE cross-sections is not exceeding 15%. The CCC calculation is close to the one-channel RPAE. The situation is completely different in Ca where the $4s$ photoionization cross-section is dominated entirely by the giant $3p \rightarrow 3d$ resonance. Unfortunately, the CCC frozen-core model cannot account for this effect. Although we did not probe explicitly the DPI channel, it is fair to assume that the inter-shell correlation would play a similar role there. This means that the present Ca results should be treated as model specific calculations and certain care should be exercised when comparing these data with experiment. In the meantime, the DPI calculations on Mg can be considered as accurate as those on Be.

The double-to-single photoionization cross-section ratio for Mg and Ca is presented in Figure 5 in comparison with unpublished preliminary results of Nagata [44]. There is a strong disagreement between the theory and experiment for both targets. The calculated ratio in Mg seems to be too low whereas the same ratio in Ca is too high as compared with the experiment. On the basis of single photoionization calculations, we can expect the CCC ratio in Mg to be accurate within 15% which is far exceeded by a nearly four-fold difference with the experiment. In the meantime, the CCC calculation on Ca is much less accurate. The inter-shell correlation which is not accounted for in the present calculation can readily explain the observed difference with the experiment.

In Figure 6 we compare the double-to-single photoionization cross-section ratios of all presently studied alkaline-earth atoms with that ratio in He. The same reduced excess energy scale is used measured in units of the ionization potential of the corresponding singly charged ion: 54.4 eV for He^+ , 18.2 eV for Be^+ , 15.0 eV for Mg^+ and 11.8 for Ca^+ [2]. The corresponding photon energy scale in eV is indicated on the top horizontal scale of each panel. On the helium plot (top left panel) we show the calculated double-to-single ratio [33] which was found in excellent agreement with the latest experimental data [35]. To test the scaling of this ratio to the electron impact ionization cross-section of the He^+ ion, we draw in the same figure the theoretical (e,2e) cross-section [36] which was found in perfect agreement with the experimental data [37, 38]. This cross-section is plotted versus the reduced excess energy and scaled to the photoionization cross-section ratio near the double ionization threshold.

As was already observed by Samson [39] and later reiterated by Wehlitz et al. [5], both curves have indeed a similar shape from the threshold up to $\Delta E \simeq 0.5$. We note, however, that the elec-

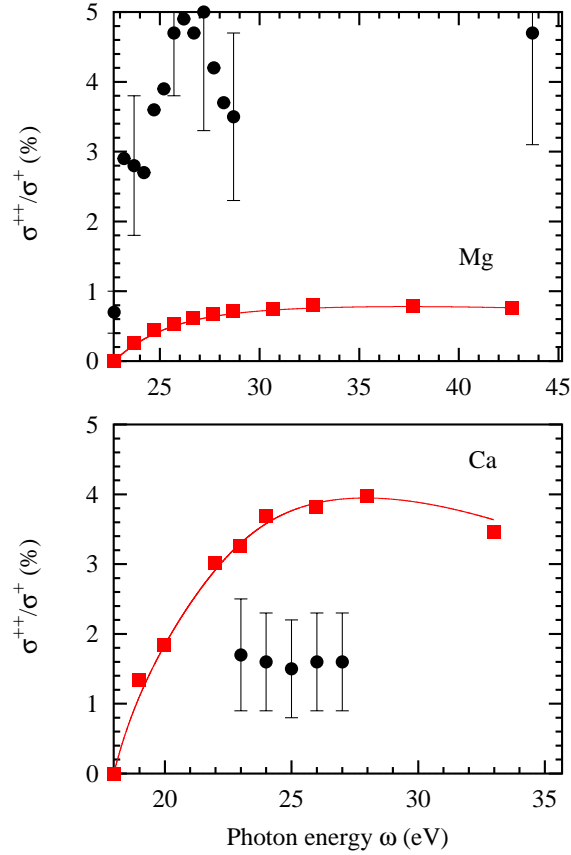


FIG. 5: Double-to-single photoionization cross-section ratios in Mg (top) and Ca (bottom) as functions of the photon energy. Present calculation (red filled squares) is shown in comparison with experimental data of Nagata [44]. The red solid line is a smooth interpolated curve to guide the eye through the calculated data.

tron impact ionization of He^+ is dominated by non-dipole partial waves which are forbidden in the photoionization process. To illustrate this fact, we present in the figure a restricted (e,2e) calculation in which all non-dipole contributions are suppressed and only the total angular momentum of the two-electron continuum $J = 1$ is allowed. To place this calculation on the common scale we have to apply a scaling factor which is 7.7 times larger than the same factor for the unrestricted (e,2e) calculation in which all J are allowed. This means that the dipole channel contributes only about 13% of the total (e,2e) cross-section. As it was argued in Ref. [40], it is this, dipole only, (e,2e) cross-section that should be scaled versus the double photoionization cross-section ratio. This scaling applies in a somewhat narrower energy range from the threshold to $\Delta E \simeq 0.3$. Out-

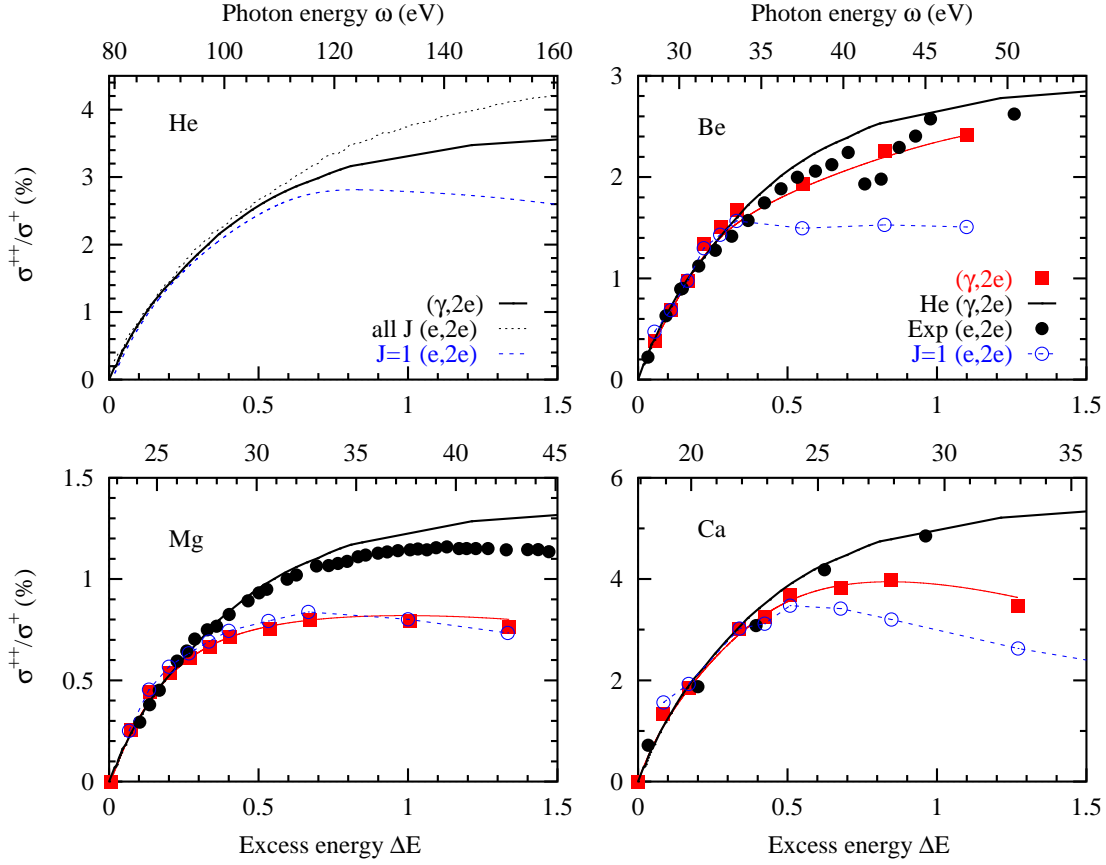


FIG. 6: Double-to-single photoionization cross-section ratios in He, Be, Mg and Ca as functions of the reduced excess energy $\Delta E = E/IP^+$ measured in units of the ionization potential of the corresponding singly charged ion. The photon energy in eV is indicated on the top horizontal scale of each plot. The data points (red filled squares) are interpolated by a smooth curve (red solid line) to guide the eye through the data. The double-to-single ratio in He [33] (multiplied by 0.8, 0.4, 1.5 to scale the Be, Mg and Ca ratios, respectively) is shown on each plot as a thick solid line. Also shown are the electron impact ionization cross-sections of the corresponding ions (CCC calculation for He [36], black dotted line; experimental data for Be [41], Mg [42] and Ca [43], filled circles) and the theoretical dipole only electron impact ionization cross-sections for each target ion (blue dashed lines)

side this range, the contribution of the other, shake-off mechanism upsets the scaling between the $(\gamma, 2e)$ and $(e, 2e)$ reactions.

Similar data presentation is used in other panels where we show the double-to-single photoion-

ization cross-section ratio for Be (top right), Mg (bottom left) and Ca (bottom right). The present calculation is compared with a scaled ratio for He [33] which is multiplied by 0.80, 0.37, 1.5 in the Be, Mg and Ca plots, respectively. The electron impact ionization of the corresponding singly charged ion is taken from experiment (Ref. [41] for Be, Ref. [42] for Mg and Ref. [43] for Ca). Dipole only (e,2e) cross-section is extracted from the same CCC calculation as the double-to-single photoionization cross-section ratio.

We observe that, in extended excess energy range up to $\Delta E \simeq 1.0$, the scaled (e,2e) cross-section on each target follows closely the double-to-single photoionization cross-section ratio of He. We can offer no explanation to this phenomenon and find it coincidental. The cross-section ratios in alkaline earth atoms follow the analogous ratio in He at excess energy range up to $\Delta E \simeq 0.3$. In Be and Ca, this is the same range where the dipole only (e,2e) cross-section scales to the photoionization cross-section ratio. In Mg, the latter scaling is extended across the whole excess energy range shown on the plot. Such a scaling indicates the range of photon energies where the electron impact ionization of the singly charged ion is the dominant mechanism of DPI. The alternative shake-off mechanism contributes insignificantly in this range.

Characteristic values of the photoionization cross-section ratios in Be and Mg at the excess photon energy range $\Delta E \simeq 1$ are smaller than in He. This goes in line with reduction of the asymptotic R_∞ ratio in this sequence of targets. However, Ca breaks away from this tendency and exhibits the double-to-single ratio greater than that in He. This could possibly be explained by an electron impact ionization cross-section on Ca^+ which is significantly larger than that on He^+ .

B. DPI amplitudes

Modulus of the symmetric amplitude f^+ of DPI on Be is shown in Figure 7 for selected excess energies of 20, 4 and 1 eV shared equally between the photoelectrons. The fit with a Gaussian ansatz Eq. (11) is also shown in the figure. The quality of the fit is very good on the middle panel with deviation from the Gaussian hardly visible on the scale of the figure. The fit somewhat deteriorates on the top and bottom panels, but for different reason. The top panel represents the amplitude taken quite far away from the DPI threshold at the reduced excess energy of $E/IP^+ = 1.1$. We note that the same excess energy of 20 eV would correspond to $E/IP^+ = 0.37$ in He. The amplitude shown on the bottom panel is taken very close to the threshold. Here, the noticeable wings of the

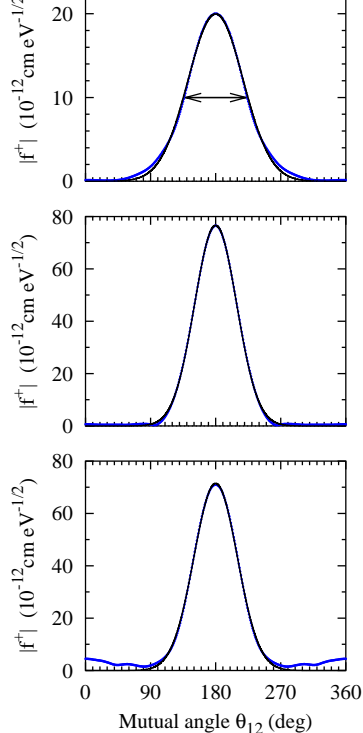


FIG. 7: Modulus of the symmetric amplitude f^+ of DPI on Be at equal energy sharings of $E_1 = E_2 = 10$ eV, 2 eV and 0.5 eV (from top to bottom). The arrow indicates the Gaussian width parameter $\Delta\theta_{12}$ in Eq. (11)

amplitude near zero mutual angle is most likely a numerical artifact. The symmetric amplitude should be zero at this angle as emission of the two equal energy electrons in the same direction is prohibited. However, in the CCC formalism, the two electrons are explicitly distinguishable. It is the full numerical convergence that assures a complete cancellation of the DPI amplitude at zero mutual angle. The excess energy of $\simeq 1$ eV represents the lower limit of the present calculation where this convergence can be confidently reached.

Although not shown in the figure, the same Gaussian shape of the symmetric amplitude f^+ can be observed in other alkaline earth atoms (Mg and Ca). This is in contrast to predictions of Kazansky and Ostrovsky [14] who reported a double hump structure of $|f^+|^2$ in all alkaline earth atoms in the range of excess energies from 0.5 to 5 eV.

The Gaussian width parameter as a function of excess energy for Be and other alkaline earth atoms is shown in Figure 8 in comparison with the width parameter of He. As in Figure 6, we use the reduced excess energy scale $\Delta E = E/IP^+$ measured in units of the ionization potential of the corresponding singly charged ion.

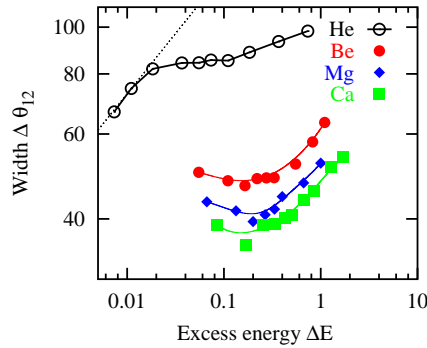


FIG. 8: Gaussian width parameter $\Delta\theta_{12}$ as a function of the reduced excess energy $\Delta E = E/IP^+$ for various alkaline earth atoms (Be, red circles; Mg, blue diamonds; Ca, green squares) and helium (black open circles). The correspondingly colored solid lines are smooth interpolated curves to guide the eye through calculated data. The dotted line indicates the onset of the Wannier threshold law $\propto E^{1/4}$ for He.

Firstly, we observe a significant reduction of the Gaussian width parameter in alkaline earth atoms as compared with He. This reduction was already reported in previous calculations on Be [6, 30]. However, the origin of this reduction was attributed to different factors. Citrini et al. [6] explained it in terms of greater ground state correlation in Be as compared to He. Conversely, it was argued in Ref. [10] that this effect had little to do with electron properties of the neutral target. Rather, it could be explained by the narrowing width of the momentum profile of the bound electron attached to the corresponding singly charged ion.

In Figure 9 we plot the momentum profiles (squared momentum space wave functions) $|R_{ns}(q)|^2$ of the valence ns states in He^+ ($n = 1$), Be^+ ($n = 2$), Mg^+ ($n = 3$) and Ca^+ ($n = 4$). All the momentum profiles are normalized to $|R_{1s}|^2$ of He^+ at its maximum. We see that, indeed, the width of the momentum profile is receding monotonously from He to Ca, hand in hand with the Gaussian width parameters in Figure 8. To quantify this reduction, we took the Gaussian width in all the targets at a fixed, somewhat arbitrarily, reduced excess energy of $\Delta E = 0.3$ and plotted it versus the momentum width at half maximum Δq extracted from the momentum profiles of Figure 9. Resulting dependence is shown in Figure 10. The calculated data points in Figure 8 are somewhat scattered. So the width parameters presented in Figure 10 are supplied with “error bars” extracted from the interpolation procedure. Within these “error bars”, the calculated points in Figure 10 can be approximated by the $\Delta\theta_{12} \propto \Delta q^{3/4}$ dependence.

In addition to the systematic reduction of the Gaussian width, we observe in Figure 8 a non-monotonous dependence of the width versus the excess energy in the alkaline earth atoms in contrast to that in He. The width, as a function of the excess energy, displays a shallow minimum at $E \approx 0.3IP^+$. This behaviour is unexpected. The Wannier threshold law for the angular correlation width is $\Delta\theta_{12} \propto E^{1/4}$ [28, 29]. The He data seem to approach the Wannier regime at quite small excess energies of the order of $E \simeq 0.01IP^+$. Other alkaline earth atoms have much smaller ionization potentials of the singly charged ions and the regime of very small $\Delta E \sim 0.01$ cannot be reached in the present calculation.

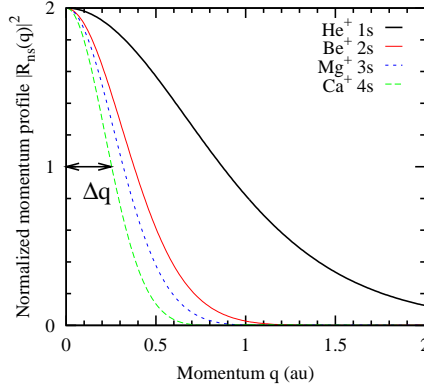


FIG. 9: Momentum profiles (squared momentum space wave functions) $|R_{ns}(q)|^2$ of the valence ns state in He⁺ ($n = 1$, black thick solid line), Be⁺ ($n = 2$, red solid line), Mg⁺ ($n = 3$, blue short dash line) and Ca⁺ ($n = 4$, green long dash line). The momentum profiles are normalized to $|R_{1s}|^2$ of He⁺ at its maximum. The arrow indicates the extraction of the momentum width at half maximum Δq .

C. Triply differential cross-section

Knowledge of the ionization amplitude allows one to generate the fully resolved TDCS for arbitrary polarization of light, geometry of two-electron escape and energy sharing between the photoelectrons. In Figure 10 (middle panel), we present the TDCS of Ca at the excess energy of 25 eV shared equally between the photoelectrons. Comparison is made with experiment of Beyer et al. [12] in which the fixed angle electrons were ejected parallel to the electric vector of 100% linearly polarized light. In the same figure (bottom panel) we present analogous TDCS results for He calculated at the same geometry. The excess energy $E = 20$ eV is chosen somewhat lower to

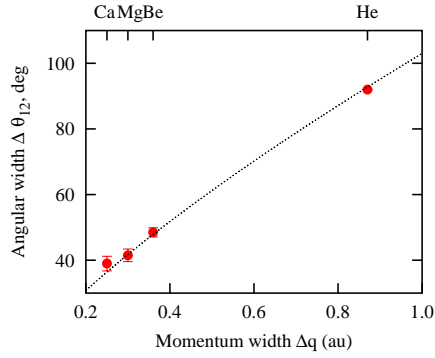


FIG. 10: Gaussian angular width parameter $\Delta\theta_{12}$ taken at the reduced excess energy $\Delta E = E/IP^+ = 0.3$ versus the momentum width at half maximum Δq in He and various alkaline earth atoms. The dotted line is fitting with the power law $\Delta\theta_{12} \propto \Delta q^{3/4}$

make a comparison with the experimental data of Bräuning et al. [45]. To facilitate analysis of the TDCS results, on the top panel of the figure we plot the symmetric DPI amplitudes of Ca and He at the corresponding excess energies. As the fixed electron is detected at zero angle $\theta_1 = 0^\circ$, the variable angle θ_2 is equal to the mutual electron angle $\theta_{12} = \theta_2 - \theta_1$ and all three plots can be aligned to the same x scale.

The symmetrized amplitude in He has a nearly perfect Gaussian shape with a width parameter of $\Delta\theta_{12} \simeq 95^\circ$. The corresponding TDCS has a single maximum at $\theta_{12} \simeq 100^\circ$. This maximum is reached as a “compromise” between the amplitude (dynamical factor) which has a maximum at $\theta_{12} = 180^\circ$ and the kinematical factor $\cos \theta_1 + \cos \theta_2$ which has a node at this angle.

The central part of the symmetrized amplitude in Ca has a Gaussian shape as well with a much narrower width parameter of $\Delta\theta_{12} \simeq 56^\circ$. The sharp peak of the amplitude at $\theta_{12} = 180^\circ$ gives rise to a maximum of the TDCS at about $\theta_{12} \simeq 135^\circ$. This is visualized by the black solid line which represents the TDCS generated from the Gaussian fit to the symmetric amplitude shown on the top panel of Figure 10. In deviation from a Gaussian, this amplitude has a little hump at $\theta_{12} \simeq 100^\circ$. This non-Gaussian feature is due to a much larger reduced excess energy of $E/IP^+ = 2.1$ as compared to only 0.36 in He which means that the Ca data are taken much further away from the threshold where the Gaussian parametrization does not hold so well. The additional feature of the amplitude gives rise to a bold maximum of TDCS at $\theta_{12} \simeq 105^\circ$. Experimental data show a single maximum which is roughly in between the two maxima on the theoretical curve. We should note that the TDCS presented in Figure 11 correspond to the photon energy of 36.8 eV which is very

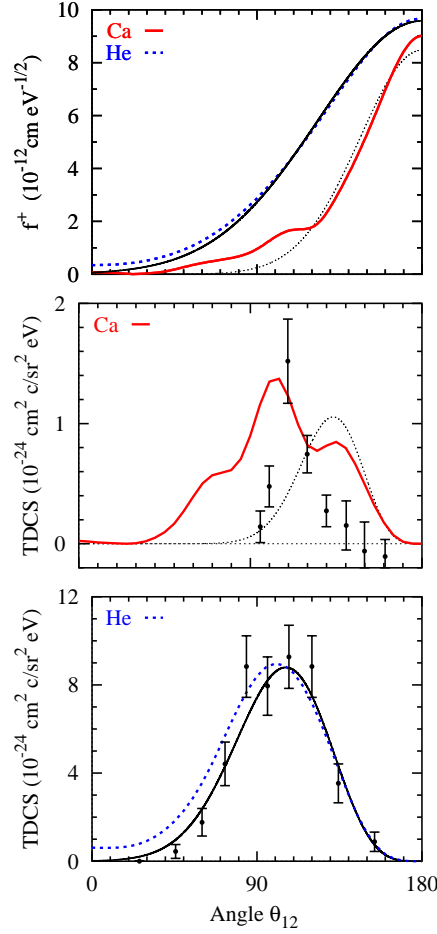


FIG. 11: Top panel: symmetric DPI amplitudes $f^+(\theta_{12}, E_1, E_2)$ at $E_1 = E_2 = 12.5$ eV in Ca (red solid line) and at $E_1 = E_2 = 10$ eV in He (blue dotted line) plotted versus the mutual electron angle θ_{12} . Both amplitudes are fitted with the Gaussian ansatz Eq. (11) shown by the black solid (He) line and dotted (Ca) lines. Middle panel: DPI TDCS of Ca at $E_1 = E_2 = 12.5$ eV at fixed electron angle $\theta_1 = 0$ plotted versus θ_{12} . Experimental data from Ref. [12] on relative scale are normalized to the calculation. Bottom panel: same for He at $E_1 = E_2 = 10$ eV. Absolute experimental data are from Ref. [45]. The black solid line on the middle panel and black dotted line on the bottom panel indicate the TDCS generated from the Gaussian fit to the corresponding symmetric amplitudes shown on the top panel.

close to the giant $3p \rightarrow 3d$ resonance at 31.4 eV which can modify strongly the present frozen-core calculation.

IV. CONCLUSION

In the present paper we report on the convergent close-coupling calculations of double photoionization of alkaline earth atoms: Be, Ca and Mg. Our model comprises the MCHF expansion of the valence shell of the target atom and the CCC expansion of the two electron continuum in the Hartree-Fock field of the ionized target. Both in the ground state and the final ionized state, the core (and subvalent) electrons are kept frozen.

As a test bench, we use the recent accurate measurement of the single and double photoionization cross-sections in Be [5]. Our data are in a reasonable agreement with experiment. For the single photoionization cross-section, the theory is about 10% below the experimental data near the DPI threshold, but comes into better agreement further away from the threshold. By relaxing the core and calculating the cross-section in the RPAE approximation, we can bring the theoretical cross-section in perfect agreement with the experiment. This kind of calculation, however, is only available for single photoionization. For double photoionization, our CCC calculation in the velocity gauge is about 20% higher than the experiment near the threshold. Agreement is somewhat better at excess energies above 10 eV.

Having tested our model, we proceed with calculations for other atoms, Mg and Ca. We use the notion of the reduced excess energy measured in units of the ionization potential of the singly ionized target. This allows us to bring alkaline earth atoms and He on the common scale. On this scale, the double-to-single photoionization cross-sections ratio in all the targets follows a universal shape function. This is related to the fact that DPI process near threshold in all two-electron targets is dominated by the electron impact ionization of the corresponding singly charged ion. The cross-section of the latter process can be scaled to a universal shape function. However, we find two important differences as compared with the earlier interpretations of Samson [39] and Wehlitz et al. [5]. Firstly, scaling of the double-to-single photoionization cross-sections ratios is observed in a much reduced excess energy range from the threshold to $\Delta E \simeq 0.3$. Secondly, it is the dipole only (e,2e) cross-section which should be taken for the electron impact ionization process.

The magnitude of the double-to-single photoionization cross-section ratio in He and alkaline earth atoms is a result of interplay of two DPI mechanisms: shake-off and (e,2e) on singly charged ion. The former process can be characterized by the asymptotic ratio R_∞ taken in the limit of infinite photon energy. This ratio is decreasing from He to Ca due to increasing probability of the

second target electron to remain bound because of a closer overlap of the neutral and ionized target orbitals. This, in turn, is caused by a shielding effect of the other core and subvalent electrons. On the contrary, the electron impact ionization cross-section of the singly charged ion is growing from He^+ to Ca^+ due to increasing size of the valence orbital in the coordinate space. These two competing tendencies result in reduction of the double-to-single photoionization cross-section ratio from He to Mg but its bouncing back in Ca.

To further our understanding of DPI process, we extract the symmetrized DPI amplitudes in alkaline earth atoms and compare them with He. We concentrate on a special case of the equal energy sharing when only one fully symmetric amplitude is needed to generate the TDCS. In the range of excess energy not exceeding the corresponding ionization potential of the singly charged ion $\Delta E = E/IP^+ \leq 1$, the amplitudes can be fitted with a Gaussian ansatz. The Gaussian width parameter in all the alkaline earth atoms studied here is much smaller than in He at the corresponding reduced excess energy. We explain this decrease by narrowing the width of the momentum profile of the valence ns orbital in the corresponding singly charged ion. This corresponds to a more diffuse orbital in the coordinate space shielded by other core and subvalent electrons from the nucleus. Alternative explanation put forward by Citrini et al. [6] cannot be ruled out because the ground state correlation is indeed stronger in alkaline earth atoms than in He. However, because of a close relation of the DPI and electron impact ionization of the singly charged ion which manifests itself in scaling of the integrated cross-sections, we would argue that the former cause is more likely than the latter.

Unlike in He, the Gaussian width parameter in the alkaline earth atoms is not a monotonous function of excess energy and has a shallow minimum at $E \approx 0.3IP^+$. This behavior is at odds with the Wannier threshold law which predicts a monotonous decrease $\Delta\theta_{12} \propto E^{1/4}$. On one hand, the observed minimum can be outside the range of validity of the Wannier law whose onset takes place in He at $E \simeq 0.01IP^+$. On the other hand, Lukic et al. [8] reported a noticeable deviation from the Wannier regime in Be in the form of an oscillating DPI cross-section which they attributed to the Coulomb-dipole field of the singly ionized target. Unfortunately, in the present study, we cannot reproduce these results because our calculation is poorly converged and lacks sufficient accuracy at very small excess energies close to the threshold.

To summarize our finding, we note that, in the excess energy range studied here, DPI of alkaline atoms resembles qualitatively that of helium. A quantitative difference is caused by the structure

of the ns valence orbital which has a two-fold effect. A more diffuse structure in the coordinate space causes a closer overlap between the target orbitals bound to the neutral atom and the singly charged ion thus increasing the chance of the target electron to remain bound and decreasing the probability of DPI. Secondly, narrowing of the momentum profile of the ns orbital bound to the singly charged ion reduces the angular correlation width in the two-electron continuum. Increasing strength of the ground state correlation from He to Be and further still to Mg and Ca may also play a role.

In addition to these qualitative differences, we observed a new quantitative effect present in DPI of alkaline earth atoms and absent in He. The correlation width parameter is not a monotonous function of excess energy and has a shallow minimum. This observation contradicts the Wannier threshold law. However, the onset of the threshold law may be at a lower excess energy range, not accessible in the present study.

We finally note that the present Ca results are obtained within the frozen core model which cannot account for the strong inter-shell correlation between the valence $4s^2$ and sub-valent $3p^6$ shells. To make theoretical predictions which can be reliably compared with experimental data, this inter-shell correlation should be included into the model. This development is now in progress.

Acknowledgments

We thank Ralf Wehlitz and Tetsuo Nagata for communicating their experimental results in numerical form. One of the authors (ASK) wishes to thank the Japan Society for the Promotion of Science for supporting his visit to the Photon Factory. He greatly values many stimulating discussions with Prof. Y. Azuma. The authors wish to thank Australian Partnership for Advanced Computing (APAC) and ISA Technologies, Perth, Western Australia, for provision of their computing facilities. Support of the Australian Research Council in the form of Discovery grant DP0451211 is acknowledged.

-
- [1] K. G. Dyall, I. P. Grant, C. T. Johnson, F. P. Parpia, and E. P. Plummer, *Comp. Phys. Comm.* **55**, 425 (1989).
- [2] A. A. Radzig and B. M. Smirnov, *Reference Data on Atoms, Molecules, and Ions* (Springer-Verlag, Berlin, 1985).
- [3] R. Wehlitz and S. B. Whitfield, *J. Phys. B* **34**, L719 (2001).
- [4] A. S. Kheifets and I. Bray, *Phys. Rev. A* **65**, 012710 (2002).
- [5] R. Wehlitz, D. Lukic, and J. B. Bluett, *Phys. Rev. A* **71**, 012707 (pages 5) (2005).
- [6] F. Citrini, L. Malegat, P. Selles, and A. K. Kazansky, *Phys. Rev. A* **67**, 042709 (2003).
- [7] J. Colgan and M. S. Pindzola, *Phys. Rev. A* **65**, 022709 (2002).
- [8] D. Lukic, J. B. Bluett, and R. Wehlitz, *Phys. Rev. Lett.* **93**, 023003 (pages 4) (2004).
- [9] A. Temkin, *Phys. Rev. Lett.* **49**, 365 (1982).
- [10] A. S. Kheifets and I. Bray, *Phys. Rev. A* **73**, 020708 (2005).
- [11] T. Osawa, Y. Tohyama, R. Kobayashi, S. Obara, Y. Azuma, and T. Nagata, in *XIV International Conference on Vacuum Ultraviolet Radiation Physics* (Cairns, Australia, 2004), pp. W-Po-28.
- [12] H.-J. Beyer, J. B. West, K. J. Ross, and A. D. Fanis, *J. Phys. B* **33**, L767 (2000).
- [13] S. C. Ceraulo, R. M. Stehman, and R. S. Berry, *Phys. Rev. A* **49**, 1730 (1994).
- [14] A. K. Kazansky and V. N. Ostrovsky, *J. Phys. B* **30**, L835 (1997).
- [15] K. J. Ross, J. B. West, and H.-J. Beyer, *J. Phys. B* **30**, L735 (1997).
- [16] K. J. Ross, J. B. West, H.-J. Beyer, and A. D. Fanis, *J. Phys. B* **32**, 2927 (1999).
- [17] A. D. Fanis, H.-J. Beyer, K. J. Ross, and J. B. West, *J. Phys. B* **34**, L99 (2001).
- [18] J. B. West, K. J. Ross, H.-J. Beyer, A. D. Fanis, and H. Hamdy, *J. Phys. B* **34**, 4167 (2001).
- [19] F. Maulbetsch, I. L. Cooper, and A. S. Dickinson, *J. Phys. B* **33**, L119 (2000).
- [20] L. Malegat, F. Citrini, P. Selles, and P. Archirel, *J. Phys. B* **33**, 2409 (2000).
- [21] A. Dalgarno and A. L. Stewart, *Proc. Phys. Soc. London* **76**, 49 (1960).
- [22] T. Pattard, *J. Phys. B* **35**, L207 (2002).
- [23] M. Y. Amusia, *Atomic photoeffect* (Plenum Press, New York, 1990).
- [24] L. V. Chernysheva, N. A. Cherepkov, and V. Radojevic, *Comp. Phys. Comm.* **11**, 57 (1976).
- [25] I. Bray and A. T. Stelbovics, *Phys. Rev. Lett.* **70**, 746 (1993).

- [26] A. Huetz, P. Selles, D. Waymel, and J. Mazeau, *J. Phys. B* **24**, 1917 (1991).
- [27] L. Malegat, P. Selles, and A. Huetz, *J. Phys. B* **30**, 251 (1997).
- [28] A. R. P. Rau, *J. Phys. B* **9**, L283 (1976).
- [29] J. M. Feagin, *J. Phys. B* **17**, 2433 (1984).
- [30] A. S. Kheifets and I. Bray, *Phys. Rev. A* **65**, 022708 (2002).
- [31] P. Bolognesi, I. Bray, A. Kheifets, L. Malegat, P. Selles, A. K. Kazansky, and L. Avaldi, *J. Phys. B* **36**, L241 (2003).
- [32] A. Knapp, B. Krässig, A. Kheifets, I. Bray, T. Weber, A. L. Landers, S. Schössler, T. Jahnke, J. Nickles, S. Kammer, et al., *J. Phys. B* **28**, 645 (2005).
- [33] A. S. Kheifets and I. Bray, *Phys. Rev. A* **58**, 4501 (1998).
- [34] J. M. Feagin, *J. Phys. B* **28**, 1495 (1995).
- [35] R. Dörner, T. Vogt, V. Mergel, H. Khemliche, S. Kravis, and C. L. Cocke, *Phys. Rev. Lett.* **76**, 2654 (1996).
- [36] I. Bray, I. E. McCarthy, J. Wigley, and A. T. Stelbovics, *J. Phys. B* **26**, L831 (1993).
- [37] B. Peart, D. S. Walton, and K. T. Dolder, *J. Phys. B* **2**, 1347 (1969).
- [38] P. Defrance, F. Brouillard, W. Claeys, and G. V. Wassenhove, *J. Phys. B* **14**, 103 (1981).
- [39] J. A. R. Samson, *Phys. Rev. Lett.* **65**, 2861 (1990).
- [40] A. S. Kheifets, *J. Phys. B* **34**, L247 (2001).
- [41] R. A. Falk and G. H. Dunn, *Phys. Rev. A* **27**, 754 (1983).
- [42] B. Peart, J. W. G. Thomason, and K. Dolder, *J. Phys. B* **24**, 4453 (1991).
- [43] B. Peart, J. R. A. Underwood, and K. Dolder, *J. Phys. B* **22**, 2789 (1989).
- [44] T. Nagata (2006), private communication.
- [45] H. Bräuning, R. Dörner, C. L. Cocke, M. H. Prior, B. Krässig, A. S. Kheifets, I. Bray, A. Bräuning-Demian, K. Carnes, S. Dreuil, et al., *J. Phys. B* **31**, 5149 (1998).